Exploring Molecular Changes at the Surface of Polypropylene after Accelerated Thermomolecular Adhesion Treatments

Firas Awaja,*,† Michael Gilbert,‡ Georgina Kelly,† Bronwyn Fox,† Russell Brynolf,§ and Paul J. Pigram‡

Centre for Material and Fibre Innovation, Geelong Technology Precinct, Deakin University Geelong, Victoria 3217, Australia, Centre for Materials and Surface Science and Department of Physics, La Trobe University, Victoria 3086, Australia, and FTS Technologies, 11084 HiTech Drive, Whitmore Lake, Michigan 48189

ABSTRACT A central composite rotatable design (CCRD) method was used to investigate the performance of the accelerated thermomolecular adhesion process (ATmaP), at different operating conditions. ATmaP is a modified flame-treatment process that features the injection of a coupling agent into the flame to impart a tailored molecular surface chemistry on the work piece. In this study, the surface properties of treated polypropylene were evaluated using X-ray photoelectron spectroscopy (XPS) and time-of-flight secondary ion mass spectrometry (ToF-SIMS). All samples showed a significant increase in the relative concentration of oxygen (up to 12.2%) and nitrogen (up to 2.4%) at the surface in comparison with the untreated sample (0.7% oxygen and no detectable nitrogen) as measured by XPS. ToF-SIMS and principal components analysis (PCA) showed that ATmaP induced multiple reactions at the polypropylene surface such as chain scission, oxidation, nitration, condensation, and molecular loss, as indicated by changes in the relative intensities of the hydrocarbon ($C_3H_7^+$, $C_3H_5^+$, $C_4H_7^+$, and $C_5H_9^+$), nitrogen and oxygen-containing secondary ions ($C_2H_3O^+$, $C_3H_8N^+$, $C_2H_5NO^+$, $C_3H_6NO^+$, and $C_3H_7NO^+$). The increase in relative intensity of the nitrogen oxide ions ($C_2H_5NO^+$ and $C_3H_7NO^+$) correlates with the process of incorporating oxides of nitrogen into the surface as a result of the injection of the ATmaP coupling agent.

KEYWORDS: polypropylene • surface modification • adhesion strength • ToF-SIMS • XPS • ATmaP

INTRODUCTION

Polypropylene (PP) is widely used in the automotive industry, and typically exhibits low surface energy and a lack of polar surface functional groups, giving rise to poor surface adhesion (1−3). A number of surface treatment processes, including the use of primers (4) and traditional flame treatment (5, 6), improve surface adhesion performance. However, the need to reduce the use of potentially hazardous chemical materials in surface treatments and to improve process consistency and reliability has prompted the development of a new processing technique addressing these issues. This surface treatment technology, termed the accelerated thermomolecular adhesion process (ATmaP), has been introduced by FTS Technologies, Michigan. ATmaP is a modified flame treatment, designed to graft an atomized and vaporized nitrogen-based coupling agent (*n*-methylpyrrolidone, C_5H_9NO) to the material surface. It has been shown that the incorporation of oxides of nitrogen in the surface of the treated material leads to better adhesion performance (7).

Previous studies have reported the use of coupling agents for surface treatments to improve adhesion (8−10). Coupling agents containing vinyl groups are reported to react with a corresponding binder but no correlation with adhesion performance has been found (10, 11). There has been no discussion in the literature as yet regarding the reaction mechanism by which these coupling agents bind to the surface.

In this work, changes in the relative concentrations of functional groups and elements as a result of the ATmaP surface treatment are investigated to elucidate the molecular bonding mechanism of adhesion. Molecular bonding is the most widely accepted mechanism to explain the adhesion behavior of two surfaces in close contact. It relies upon intermolecular forces between adhesive and substrate such as dipole−dipole interactions, van der Waals forces, and chemisorption (that is, ionic, covalent, and metallic bonding). This mechanism describes the strength of the adhesive joints by interfacial forces and by the presence of polar groups (12).

ToF-SIMS is a powerful and sensitive surface analysis technique that provides information about surface composition, molecular structure, and chemical bonding (13−17). ToF-SIMS data sets are information-rich. However, matrix effects and the complexities of the ionization processes occurring make quantification difficult. Quantitative information may be extracted in some cases with the use of standards and well-defined matrices.

* Corresponding author. Present address: School of Physics, University of Sydney, Sydney 2006, NSW, Australia. E-mail: firas@physics.usyd.edu.au.
Received for review February 16, 2010 and accepted April 16, 2010
† Deakin University Geelong.
‡ La Trobe University.
§ FTS Technologies.
DOI: 10.1021/am1001376

Table 1. Coded Values vs Real Values

	coded values				
	−1.73	−1	0	1	1.73
x1	0	0.43	0.75	1.18	1.5
x2	0	7.2	12.5	19.7	25
x3	0	2.3	4	6.3	8

The complexity of ToF-SIMS data necessitates the use of data pretreatment methods and multivariate analysis (MVA) tools such as principal components analysis (PCA) to provide meaningful information. A number of groups have developed the use of multivariate calibration for analyzing ToF-SIMS data (14, 18−20). Wagner et al. (19) reviewed a range of previous work, highlighting the data pretreatment processes and the multivariate analysis techniques that have been used with different organic materials systems. Graham et al. (14) explained some of the conventional data pretreatments and the challenges facing the use of the multivariate analysis (MVA) with ToF-SIMS data. Surface chemical information from techniques such as XPS is complementary to data derived from ToF-SIMS and is widely used in combination to explain surface molecular characteristics. Médard et al. (21) used XPS data (obtained at 90° takeoff angles) and ToF-SIMS data to show strong agreement between indicators of surface functionalization from both techniques in response to CO_2 plasma treatment of polypropylene

XPS may be used to identify bonding conditions via spectral features such as chemical shifts and resonance effects in core level photoelectron spectra. XPS provides quantitative surface composition information via the use of photoelectron peak intensities and corresponding semiempirical relative sensitivity factors.

ATmaP process have been examined previously and found to improve adhesion strength significantly in comparison with conventional flame treatments (22). Surface inspection showed an increase in oxygen and nitrogen concentration on the surface of ATmaP-treated samples compared with untreated and flame-treated samples as measured by XPS. ToF-SIMS analysis revealed that main events are chain scission of the PP backbone chain and the subsequent reaction of these chains with the surrounding air. ToF-SIMS also revealed an increase in the concentration of NO surface functional groups as a result of ATmaP process.

An experimental design is necessary to cover the ATmaP process variables with an optimum number of experiments. A central composite rotatable design (CCRD) method was used in this study; it provides a reasonable distribution of data throughout the region of interest and does not require a large number of experiments. CCRD also allows for an efficient optimization procedure to predict the highest concentrations of oxygen and nitrogen elements on the treated surfaces. The theory and practice of CCRD have been reported elsewhere (23).

In this article, we present the results of the investigation of the ATmaP process parameters using a CCRD experimental design method and the effect of these parameters on surface properties of polypropylene. XPS and ToF-SIMS have been used to evaluate surface properties after different ATmaP treatments.

EXPERIMENTAL SECTION

Materials. Polypropylene panels (EPALEX, PolyPacific Pty Ltd., Australia) were surface modified using three different treatments; flame, flame and water, and ATmaP, at the industrial facilities of FTS Technologies.

ATmaP Surface Treatment Process. FTS Technologies has developed the ATmaP surface treatment process by combining a flame treatment process with another process that involves the injection of vaporized coupling agent solution. The flame treatment consists of gas burner of a novel design (termed Cirqual) that generates a natural gas or propane flame (7). The selection of the ATmaP process parameters for the experimental design was based on certain criteria including previous experience and preliminary work. The oxygen flow to the flame may be independently controlled and it is selected as the first

Table 2. Experimental Design

experiment	x1 (coded)	x2 (coded)	x3 (coded)	oxygen flow (vol %)	chem. conc. (vol %)	fluid flow rate (mL/min)
1	−1	−1	−1	0.43	7.2	2.3
2	1	−1	−1	1.18	7.2	2.3
3	−1	1	−1	0.43	19.7	2.3
4	1	1	−1	1.18	19.7	2.3
5	−1	−1	1	0.43	7.2	6.3
6	1	−1	1	1.18	7.2	6.3
7	−1	1	1	0.43	19.7	6.3
8	1	1	1	1.18	19.7	6.3
9	−1.73	0	0	0.0	12.5	4.0
10	1.73	0	0	1.5	12.5	4.0
11	0	−1.73	0	0.75	0.0	4.0
12	0	1.73	0	0.75	25.0	4.0
13	0	0	−1.73	0.75	12.5	0.0
14	0	0	1.73	0.75	12.5	8.0
15	0	0	0	0.75	12.5	4.0
16	0	0	0	0.75	12.5	4.0
17	0	0	0	0.75	12.5	4.0
18	0	0	0	0.75	12.5	4.0

Table 3. Relative Atomic Concentrations of Elements Present in the Surface of Polypropylene after Different ATmaP Treatment Conditions Determined by XPS

sample	C[a]	O	N	S 2p	Si 2p	O/C
1	89.5	8.3	2.1	0	0.2	0.093
2	87.2	11.7	1	0	0.2	0.134
3	86.4	12.2	1.2	0	0.2	0.141
4	87.4	11.6	1	0	0	0.133
5	88.3	9.4	2.2	0	0.2	0.106
6	90.4	8.9	0.5	0	0.2	0.098
7	87.1	10.6	2.2	0	0.1	0.122
8	89.6	8.3	2	0	0.1	0.093
9	88.3	9.3	2.4	0	0.1	0.105
10	89.1	9.3	1.6	0.1	0	0.104
11	85.6	11.8	1.9	0.1	0.7	0.138
12	88	10.4	1.3	0	0.2	0.118
13	88.3	10.6	0.4	0.2	0.4	0.120
14	86.7	11.5	1.7	0.1	0.1	0.133
15	89.1	10.2	0.8	0	0	0.114
16	88.6	10.3	1	0	0	0.116
17	89.3	9.9	0.8	0	0	0.111
18	89.9	9.2	0.9	0	0	0.102

[a] The standard deviation for C was 0.3 from three replicated specimen for each sample. The standard deviation of the 4 replicates samples are 0.53 (C), 0.5 (O), and 0.1 (N).

experimental parameter in the investigation using a range from 0.0 to 1.5% by volume. The coupling agent compound volume percentage in solution with water is selected as the second experimental parameter. The chemical solution is atomized into the flame via an internal mix spray gun, located in the center of the Cirqual burner. The highly modified spray gun generates low velocities with significant atomization. The highly atomized liquid is then vaporized within the flame and generates nitrogen-based functional groups which in turn are carried to the surface of the material by the flame. Because the effect of the coupling agent on the treated surfaces is dependent not only on its solution concentration but also on flow rate, the diamine solution volumetric flow rate is selected as the third and final experimental parameter in the investigation. All other process parameters such as burner distance from the surface and the application speed are kept constant at all times.

Experimental Design. The CCRD method was used to design the experiments with the three chosen ATmaP process parameters. The experimental vector (X) contains these three variables. The first variable (x_1) represents the percentage of the oxygen flow by volume to the burner in the range 0−1.5%. The second variable (x_2) is the concentration of the coupling agent in aqueous solution in the range 0−25 vol %. The third variable (x_3) represents the coupling agent solution flow rate in mL/min, ranging from 0 to 8 mL/min. An experiment with 0% coupling agent means that ATmaP is operating as a flame and water treatment only. Similarly, an experiment with 0% fluid flow indicates that ATmaP is operating as a flame treatment only.

The number of required experiments for the CCRD design may be determined from the equation

$$N = k^2 + 2k + a \quad (1)$$

where N is number of experiments, k is the number of variables, and a is the number of repetition experiments. For example, for $k = 3$ and $a = 3$, 18 experiments are required. The experimental design was selected to cover all the operational ranges. Within this range of variables, a flame-only process is one in which no fluid is dispensed (e.g., Experiment 13), and a flame and water process is one in which no chemical is added to the water fluid input (e.g., Experiment 11).

The initial step in CCRD is to set up the relationship between the coded x-scales and the real x-scales values as explained in eq 2

Table 4. Relative Atomic Concentrations of Carbon and Oxygen Species Determined from Curve-Fitting of High Resolution C 1s and O 1s XPS Spectra Obtained from Polypropylene after Different ATmaP treatment conditinos

	C 1s[a]				O1s		
sample	C−C/H	C−O/C−−N	C═O	O−C═O/N−C═O	C−O	C═O	O−C═O
1	75.2	10.6	4.2	1.2	4.7	2.1	1.9
2	69.8	12.6	3.8	2.2	5.8	3.0	2.7
3	66.5	13.0	3.0	2.3	8.8	4.2	2.2
4	69.5	12.9	4.2	2.4	5.2	3.4	2.6
5	65.1	16.8	4.3	2.8	5.3	3.2	2.5
6	73.6	12.5	2.8	2.0	4.5	2.3	2.2
7	67.9	13.2	4.6	1.8	8.1	2.5	1.8
8	72.8	11.7	3.1	2.0	6.6	2.2	1.6
9	67.2	13.4	3.6	2.8	6.8	3.8	2.5
10	69.8	13.8	3.4	2.2	6.0	2.6	2.3
11	62.6	17.4	4.7	2.6	6.0	4.0	2.7
12	68.8	13.4	3.5	2.4	6.9	3.0	2.0
13	64.4	18.9	4.7	3.1	5.0	2.1	1.9
14	63.6	14.7	5.4	2.7	6.3	4.2	3.0
15	71.7	12.9	3.8	1.6	5.8	2.6	1.5
16	69.6	15.1	3.8	2.0	6.6	1.6	1.4
17	72.2	13.0	3.6	1.4	6.8	1.9	1.1
18	72.9	14.0	3.2	1.3	5.7	1.5	1.5

[a] The standard deviation for C−C/H was 0.2 from three replicated specimen for each sample. The standard deviation of the 4 replicates samples for the C 1s functional groups are 1.42 (C−C/H), 1.02 (C−O/N) 0.28 (C═O), and 0.3 (O−C═O/N). The standard deviation of the 4 replicates samples for the O 1s functional groups are 0.55 (C−O), 0.5 (C═O), and 0.19 (O−C═O).

$$x = \frac{x_{\text{actual}} - x_{\text{centre}}}{\frac{x_{\text{centre}} - x_{\text{minimum}}}{\sqrt{k}}} \qquad (2)$$

The relationship between the coded and real variable is reported in Table 1. Table 2 shows the experimental design set for three variables.

XPS. XPS measurements were performed using an Axis Ultra DLD spectrometer (Kratos Analytical, UK), equipped with a monochromatised X-ray source (Al Kα, $h\nu = 1486.6$ eV) operating at 150 W. The spectrometer energy scale was calibrated using the Au $4f_{7/2}$ photoelectron peak at binding energy (E_B = 83.98 eV). Survey spectra were acquired for binding energies in the range 0 to 1400 eV, using a pass energy of 160 eV. The photoelectrons were collected at a takeoff angle (with respect to the analyzer axes) of $\alpha = 90$ °C 1s region spectra were acquired at a pass energy of 20 eV to obtain higher spectral resolution. Peaks were fitted with synthetic Gaussian (70%)−Lorentzian (30%) components using the Marquardt−Levenberg fitting procedure of CasaXPS and were quantified using relative sensitivity factors supplied by the spectrometer manufacturer. Linear background subtraction was used and the spectra were charge corrected by setting the C 1s C−C/H component to 285.0 eV (24). The analysis area was 700 μm × 300 μm. The relative atomic concentrations of the elements detected at the polypropylene ATmaP-treated surfaces, under different conditions, were quantified using the areas of peaks in the survey spectra and relative sensitivity factors provided by the instrument manufacturer.

ToF-SIMS. Samples from the experimental design (18 samples) were analyzed with ToF-SIMS. Analyses were performed using a ToF-SIMS IV instrument (Ion-TOF GmbH, Germany) equipped with a reflectron time-of-flight mass analyzer, a Bi cluster ion source (25 keV, Bi_3^+ ions selected) and a pulsed electron flood source for charge compensation. The primary pulsed ion beam current was 1.1 pA and the primary ion dose density was below the static SIMS limit of 10^{13} ions cm^{-2}. Positive high mass resolution (>7500 at $m/z = 30$) spectra were acquired from a minimum of three 100 μm × 100 μm areas from each sample using a cycle time of 100 μs. Positive spectra then were collected and organized in a matrix for further processing (normalization and scaling) and PCA analysis.

Data Analysis. Multiple strategies were used for selecting ToF-SIMS peaks to be included in the data matrix. Initially, peaks were selected on the basis of reference libraries and previous assignment in the literature for polypropylene and surface treated polypropylene (25−27). Peaks were also assigned by using the library and the exact mass calculator tool in the Ionspec software (Ion-TOF GmbH, Germany) to identify contaminant peaks, the hydrocarbon peaks, and peaks that were likely to correspond to fragments of the flame treatment that were not listed in the literature. Eventually, the overwhelming majority of the significant peaks above baseline in the m/z range from 0−300 that were clearly resolved were selected. The mass spectra were calibrated using a series of hydrocarbon (C_xH_y) peaks up to $m/z = 105$.

The data was grouped in a matrix and the columns in the matrix were normalized to the total intensity. The matrix was mean-centered before use in principle components analysis (PCA). PCA was performed using code developed in-house based on the covariance method algorithm described in detail by Martens and Naes (28).

Modeling. The relative atomic concentrations of oxygen, nitrogen and C═O functional groups at the surface of the treated polypropylene samples, as determined by XPS, and $C_3H_7NO^+$ relative ion intensity on the surface as determined by ToF-SIMS are considered for modeling. The model fittings require a test of significance to determine the accuracy of the fit. Different statistical tests including t and F statistics were used to test the significance of each model (23). The models and coefficients statistics including p-value, F and t tests, goodness of fit, and standard error were evaluated to optimize the selection of best fitting model.

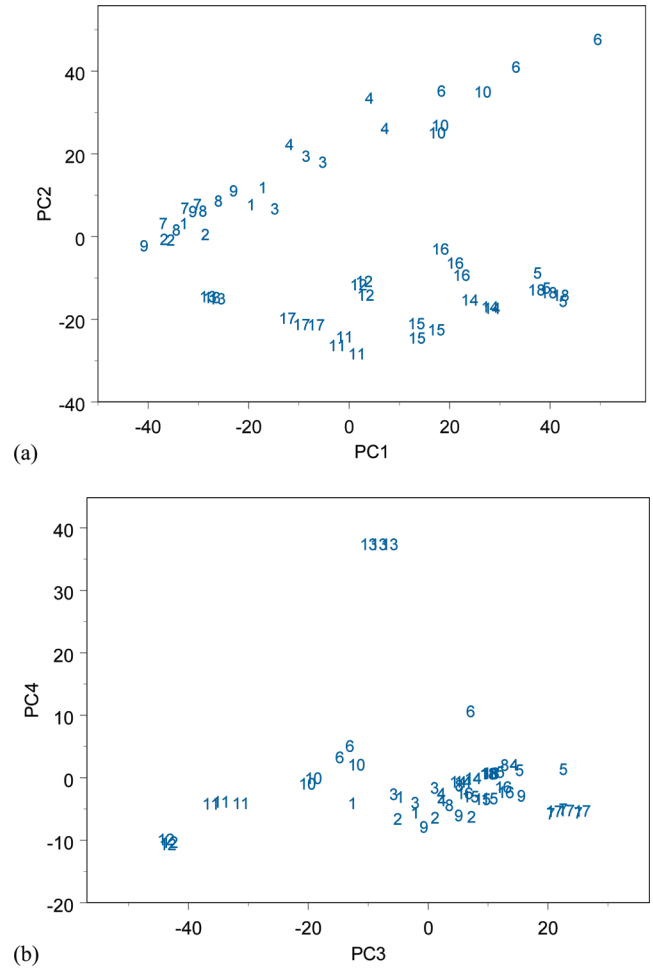

FIGURE 1. Principal component analysis score plot of (a) PC1 vs PC2 and (b) PC3 vs PC4.

RESULTS AND DISCUSSION

XPS. The surface composition data for ATmaP-treated PP, under different conditions, are presented in Table 3. Significant variations in the relative atomic concentrations of carbon, oxygen and nitrogen are observed. The lowest relative atomic concentration for carbon (85.6%) and the highest concentration for oxygen (12.20%) occur for Samples 11 and 3, respectively. Sample 3 (as shown in Table 2) was treated using low values for oxygen and fluid flow and a mid to high-range value for chemical concentration. Sample 11, corresponding to a flame and water treatment, shows a high rate of chain scission (22). Sample 9 showed the highest relative concentration for nitrogen (2.41%) as a result of process variables including the least amount of oxygen flow and midrange values for both chemical concentration and fluid flow rate. The XPS analysis of the untreated sample showed that the surface contains 99.3% carbon, 0.7% oxygen with no detectable nitrogen.

The curve fitted C 1s component peaks and corresponding relative intensities are listed in Table 4. A characteristic

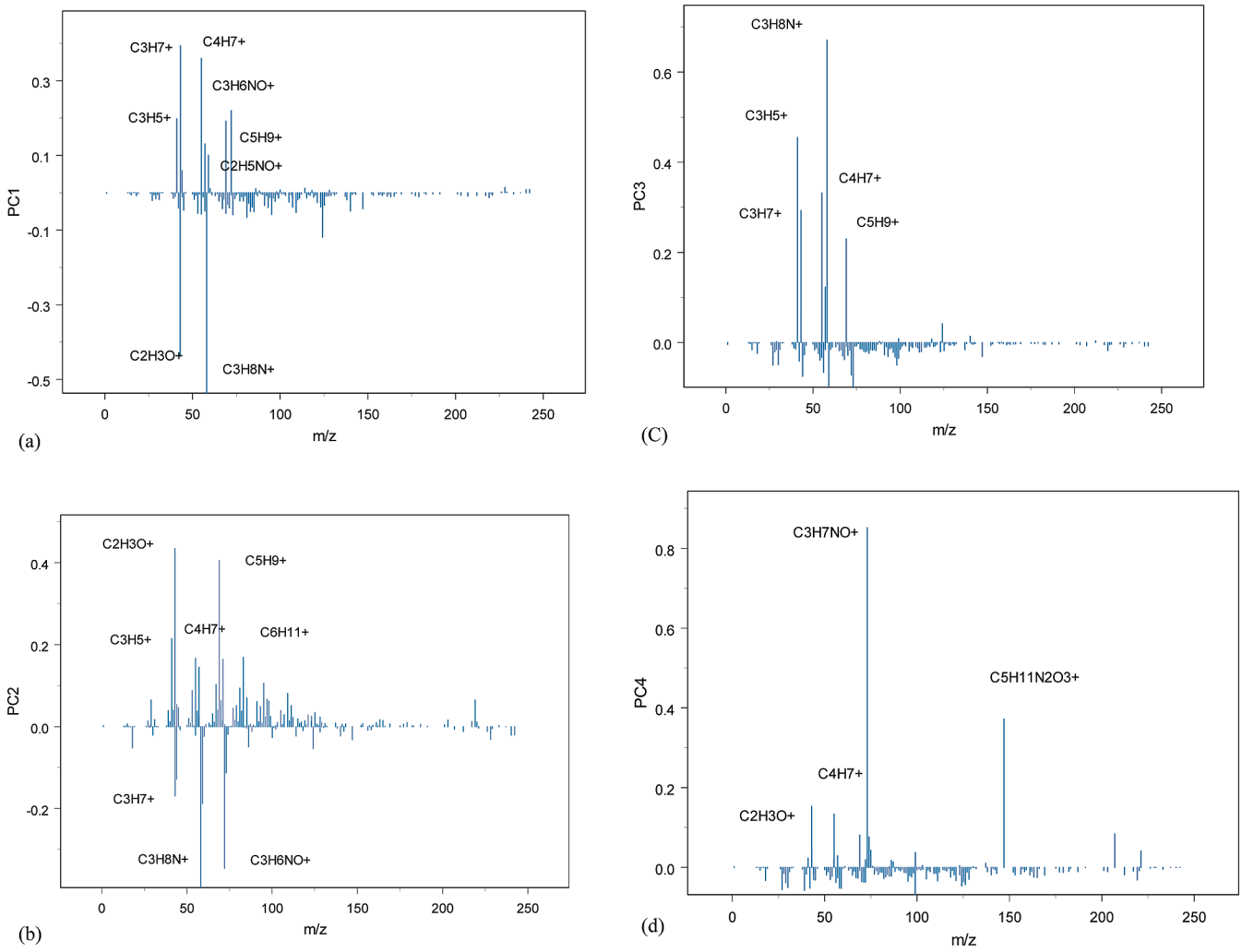

FIGURE 2. Principal components analysis loadings plots of (a) PC1, (b) PC2, (c) PC3, and (d) PC4

hydrocarbon component for the polypropylene structure was fitted to the spectra of all samples. C 1s curve fits are each consistent with the levels of oxygen and carbon detected in the corresponding survey scans; components fitted were carbon singly bonded to oxygen and to nitrogen (C—O, C—N) at approximately 286.1 eV, and carbon double bonded to oxygen (C═O) at approximately 288.0 eV. Each sample showed a high binding-energy shoulder that indicates appearance of oxygen-containing functional groups at the surface. The shoulder in all cases is fitted with a component peak attributed to O—C═O and N—C═O species at approximately 289.0 eV. Significant differences in the relative concentration of the C 1s components are observed (Table 4) that correlate with the variations in oxygen and nitrogen incorporation observed in the survey scans.

The O 1s spectra of all samples were fitted with O—C and O═C components at approximately 532.6 and 532.3 eV, respectively. The ATmaP surface treatment increased the high binding energy shoulder indicating the presence of the functional group O—C═O at 533.7 eV. The N 1s spectra of all samples showed a single component with a binding energy consistent with N—C and N—C═O species at 401.4 eV.

It has been previously identified (22) that multiple reactions such as chain scission, oxidation, nitration, cross-linking/condensation occur on the surface of polypropylene treated with ATmaP. Changes in ATmaP conditions result in different rates for the reaction types described above. The quantity and type of volatiles released as a result of the chain scission reaction also varies. Samples with a higher O/C ratio are associated with high oxidation reaction rates (Table 3). Samples with the lowest concentrations for C—C/C—H species are associated with the highest incidence of chain scission. Conversely, samples with higher concentrations of C—C/C—H species have undergone condensation and cross-linking reactions but lower rates of chain scission. The comparison between the oxygen and nitrogen species concentrations on the surface of the treated samples, Tables 3 and 4, indicates nitrogen and oxygen implantation by ATmaP flame treatment (29). The flame (exp 13) and flame and water (exp 11) produced high concentrations for oxygen and nitrogen species, and C—O and C═O functional groups, previously linked with better adhesion. It should be noted that ATmaP-treated PP exhibits even stronger adhesion performance than the flame and flame-and-water treatment (22).

ToF-SIMS. PCA was conducted on the ToF-SIMS data matrix to compress the large number of variables (peaks) to fewer components. The first (PC1), second (PC2), third (PC3), and fourth (PC4) principal components accounted for 42.98, 22.97, 19.87, and 6.25% of the total variance, respectively. The remaining principal components accounted for less than 8% of the variance and were ignored in the analysis.

Figure 1a shows the scores plot for PC1 vs PC2 which accounted for 66% of the variance. Samples 5, 11, 12, 13, 14, 15 (and the repeat Samples, 16, 17, 18) are shown clearly as a separate group and located in a cluster apart from the rest of the samples. The remaining samples show a trend in PC1 and PC2, which starts at the bottom with Sample 9 then follows the sequence of 2, 7, 8, 9, 1, 3, 4, 10, 6, hence forming the second cluster of samples.

Figure 2a shows the loadings plot for PC1. There are notable contributions from the aliphatic hydrocarbon ions $C_3H_7^+$, $C_4H_7^+$, and $C_3H_5^+$. Other contributions from $C_2H_3O^+$ and $C_3H_8N^+$ ions occur. The aliphatic hydrocarbons and the $C_2H_3O^+$ and $C_3H_8N^+$ ions appear in opposite directions in the loading plots indicating two different chemical phenomena. The aliphatic hydrocarbon ions correlate to PP backbone chain scission resulting from flame treatment while the oxygen and nitrogen-containing ions correlate with the subsequent reactions of treated surfaces with the coupling agent and the surrounding air. There is also a contribution from the nitrogen and oxygen containing ions of $C_3H_6NO^+$ and $C_2H_5NO^+$. These ions also appear in the opposite direction to the direction of the $C_2H_3O^+$ and the $C_3H_8N^+$ ions, again indicating the occurrence of two different chemical phenomena. This translates to the fact that the coupling reaction of NO functional groups has an inverse relationship with the oxidation and nitration reaction with the surrounding air (22). The loadings plot for PC2 (Figure 2b) shows that the main contribution is represented by the $C_3H_8N^+$ ion. Further contributions are observed from the $C_3H_6NO^+$ and $C_2H_3O^+$ molecular ions, as well as the aliphatic hydrocarbon ions of $C_5H_9^+$, $C_3H_5^+$, $C_3H_7^+$, and $C_6H_{11}^+$. Figure 3 shows the variation in intensity of these significant ions, selected according to the PCA outcome.

Figures 1a, 2a, and 3a show that samples in PC1 are separated mainly due to the changes in the relative ion concentration of the $C_3H_7^+$ ion. Figure 3a shows that most samples (apart from Samples 11, 12 and 13) have significant relative ion intensity for aliphatic hydrocarbon ions. This indicates that significant PP backbone scission resulted from the ATmaP treatment at the many different conditions. Samples 11, 12, and 13 showed the least evidence for PP backbone scission and the accompanying N, O and NO surface functional groups. These samples exhibit cross-linking or condensation reactions at the surface (22).

The second cluster trend is related to the relative ion concentrations of the aliphatic hydrocarbon ions especially $C_4H_7^+$ ion and nitrogen and oxygen-containing ions. As the trend moves upward, samples showed higher $C_4H_7^+$ and lower $C_3H_3O^+$ and $C_3H_8N^+$ relative ion concentrations. This

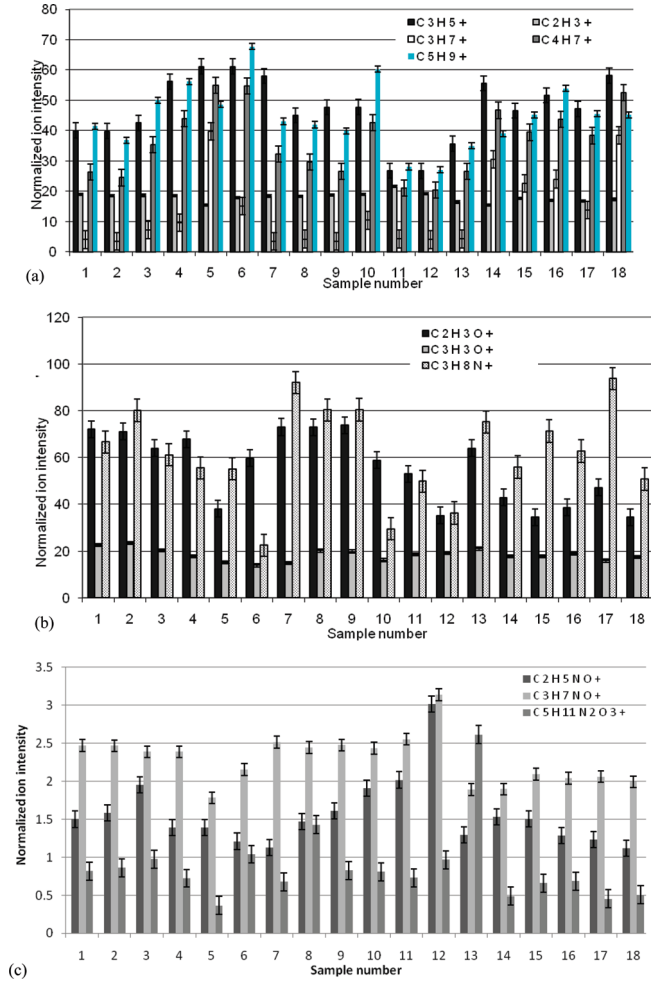

FIGURE 3. Variation in the intensity of secondary ion peaks of the samples that showed significant variance by PCA: (a) aliphatic hydrocarbon ions, (b) $-N^+$ and $-O^+$ ions, and (c) $-NO^+$ ions

is an indication of two separate chemical reactions, on the one hand chain scission and on the other oxidation and nitration, that occur at different rates for each sample in this cluster. The samples from Cluster 1 have no significant differences between the relative ion concentrations of the above ions. Hence, these samples appear to be having opposing reactions in equilibrium. Table 3 shows that samples with high nitrogen concentration at the surface, as measured by XPS, also showed a high relative ion intensity for the $C_3H_8N^+$ ion, indicating the molecular character of the nitrogen present.

Samples in Cluster 1 (Samples 5, 11,12, 13, 14, 15, 16, 17, 18) are distinguished from samples in Cluster 2 in PC2 because of the higher relative ion intensity of the nitrogen and oxygen-containing ions, as shown in Figure 3c. The increase in the $C_3H_6NO^+$ relative ion intensity is found to correlate proportionally to adhesion strength (22). Close inspection of the samples that showed a high concentration of NO^+ ions is observed for a combination of conditions including a middle to low range use of oxygen in-flow and chemical concentration, whereas fluid flow rate did not appear to make a significant contribution to variation in surface chemistry. In summary, PC2 collects information

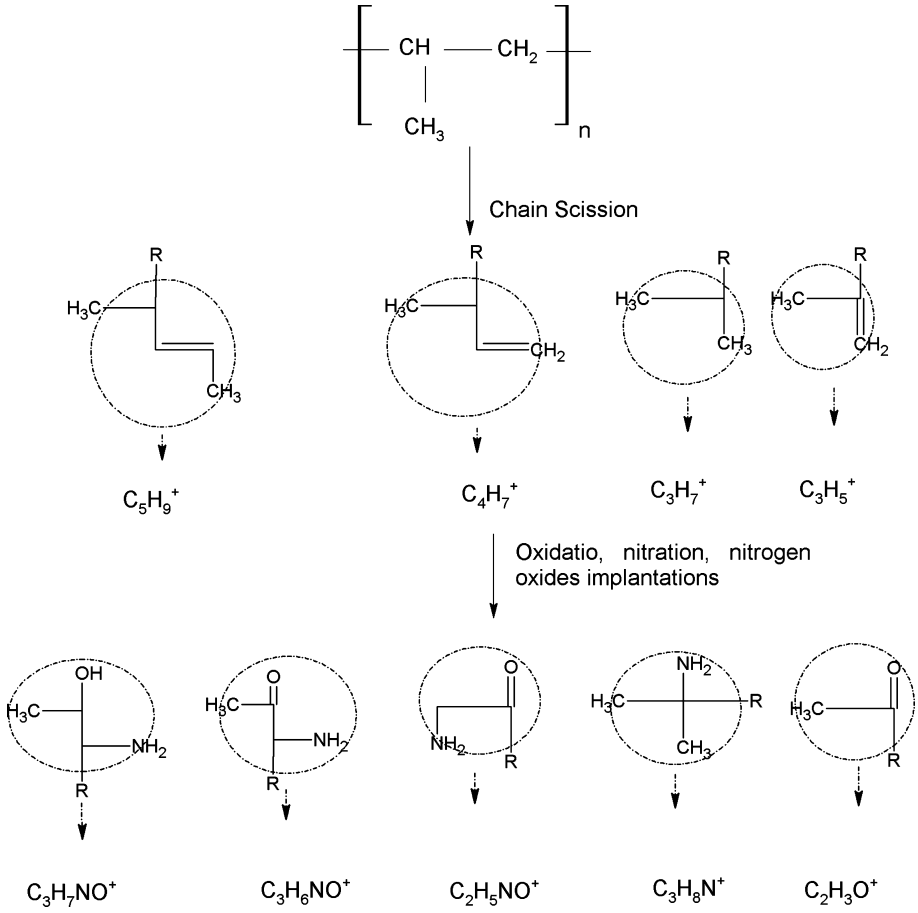

FIGURE 4. Proposed chain scission, oxidation, nitration, and implantation of nitrogen oxide mechanism according to one theme extracted from ToF-SIMS data.

that is directly related to the concentration of the NO functionality on the surface.

Figure 1b shows the score plots for PC3 vs PC4. PC3 collects information that shows a trend starting from Samples 12 and 11 and ending with Samples 4, 5 14, 15 (and the repeat samples 16, 17, and 18). Figure 2c shows the loadings plot for PC3, highlighting significant contributions from the $C_3H_8N^+$, $C_3H_5^+$, $C_4H_7^+$, $C_3H_7^+$, and $C_5H_9^+$ molecular ions. Figures 3a and 3b show that the trend collected by PC3 relates to the relative ion concentration of the $C_3H_8N^+$ ion and to the other aliphatic hydrocarbon ions to a lesser extent. Samples 11 and 12 showed least relative ion concentration of $C_3H_8N^+$ and $C_3H_5^+$ ions while the other samples showed higher concentration of these ions and organized in the trend according to their collective concentration. Information collected by PC4 reveals an outlier sample (Sample 13). Comparison between Figures 1b, 2d, and 3c shows that Sample 13 shows significantly higher $C_5H_{11}N_2O_3^+$ relative ion concentration than the rest of the samples. This indicates a direct relationship between the relative concentration of this ion and the oxygen injection to the ATmaP process since sample 13 was treated without water and coupling agent.

These results indicate two distinct and competing chemical phenomena occur in the samples as a result of ATmaP treatment. The significance of these phenomena in each sample depends on the ATmaP surface treatment conditions. The first phenomenon is the generation of NO functional groups as a result of the deposition of the atomized and vaporised coupling agent molecules on the treated surfaces. This phenomenon is evident in the rise of the relative ion intensity of the oxygen and nitrogen-containing ions ($C_xH_yNO^+$). The second phenomenon is a combination of polypropylene chain scission and subsequent reactions with air. This phenomenon is evident from the rise of relative ion intensity of the aliphatic hydrocarbon, nitrogen-containing and oxygen-containing ions ($C_2H_3O^+$, $C_3H_8N^+$). The first phenomenon is dominant in the first cluster of samples, whereas the second phenomenon is dominant in the second cluster of samples. Figure 4 shows a proposed chain scission, oxidation, nitration and generation of nitrogen oxide mechanism for the ATmaP-treated samples according to ToF-SIMS PCA analysis described above.

Model Fitting. The generation of models that represent the different molecular functionalities of the surface is an important step toward system representation. Further these models could be used in the construction of the objective functions that could be used for optimization. Polynomial models are easy to fit and have good approximations; therefore, they were selected to fit the experimental results response. A statistical analysis has been conducted to evaluate the best model for each of the parameters, as described below.

Table 5. Statistical Analysis of eq [6,a]

	value	std error	*t* value	Pr(>|*t*|)
(intercept)	16.205	3.179	5.0976	0.0014
x_1	5.6795	1.3363	4.2503	0.0038
x_2	−1.977	0.4628	−4.2715	0.0037
x_3	−1.8389	0.8077	−2.2766	0.0569
x_2^2	0.1192	0.0223	5.3406	0.0011
x_3^2	0.0831	0.0299	2.7819	0.0272
x_2^3	−0.0013	0.0004	−3.1924	0.0152
x_2x_3	0.3206	0.1084	2.9579	0.0212
x_1x_3	−0.8973	0.2759	−3.2527	0.014
$x_1x_2^2$	−0.0105	0.0032	−3.2836	0.0134
$x_3x_2^2$	−0.0131	0.0039	−3.3461	0.0123

[a] Model statistics: residual standard error, 0.5883 on 7 degrees of freedom; multiple R^2, 0.9035; F-statistic, 6.55 on 10 and 7 degrees of freedom, the *p*-value is 0.01031.

Oxygen Relative Concentration on the ATmaP Surface-Treated Samples. Oxygen relative atomic concentration at the surface of the polypropylene samples, derived from XPS, was selected as one of the optimization procedure parameters. Oxygen concentration plays a vital role in the adhesion performance of the surface and is directly affected by the ATmaP treatment process (22) as shown in Table 3.

The selected model for oxygen relative concentration $F(X)_1$ on the surface is reported in eq 6 and Table 5 shows the statistical analysis of the model

$$F(X)_1 = 16.205 + 5.6795x_1 - 1.977x_2 - 1.8389x_3 + 0.1192x_2^2 + 0.0831x_3^2 - 0.0012x_2^3 + 0.3206x_2x_3 - 0.8973x_1x_3 - 0.0105x_2^2x_1 - 0.0131x_2^2x_3 \quad (6)$$

Nitrogen Relative Concentration on the Surface. Nitrogen relative atomic concentration, also derived from XPS, was used as another parameter in the optimization procedure. It was observed that ATmaP process performance is directly related to the quantity of nitrogen functional groups at the surface (22), as shown in Table 3. Hence maximum nitrogen concentration at the surface within the working conditions is desired. Equation 7 shows the fitting model of the XPS experimental results for the relative concentration of nitrogen $F(X)_2$ and Table 6 shows the statistical analysis of the fitted model.

$$F(X)_2 = 5.4525 - 4.3264x_1 - 0.3186x_2 - 0.17x_3 + 0.0046x_2^2 + 0.8897x_1^3 + 0.1245x_1x_2 + 0.0235x_2x_3 \quad (7)$$

The nitrogen and oxygen models allow for the tailoring of the ATmaP process to achieve the desired oxygen and nitrogen relative concentration on the treated surfaces. Figure 5 shows that maximum oxygen concentration region (17−18%) is achieved at highest chemical concentration (>22%) and low solution flow rate (>1 mL/min). A separate validation sample was ATmaP treated at conditions within the described maximum oxygen range. XPS measurements showed that relative oxygen concentration on the surface is 16.4%. At chemical concentrations lower than 18%, no significant effect is noticed for the solution flow rate and the oxygen concentration is proportional to the chemical concentration. At chemical concentrations higher than 18%, the oxygen concentration is dependent on both variables. It increases with increasing chemical concentration and decreasing solution flow rate. The water component in the solution is reducing the ability of the surface to bond to oxygen functional groups.

Table 6. Statistical Analysis of eq [7,a]

	value	std error	*t* value	Pr(>|*t*|)
(intercept)	5.4525	0.597	9.1329	0.0000
x_1	−4.3264	0.5892	−7.3432	0.0000
x_2	−0.3186	0.0507	−6.2865	0.0001
x_3	−0.17	0.0911	−1.8653	0.0917
x_2^2	0.0046	0.0012	3.7579	0.0037
x_1^3	0.8897	0.1518	5.8627	0.0002
x_1x_2	0.1245	0.0354	3.5121	0.0056
x_2x_3	0.0235	0.0066	3.5325	0.0054

[a] Model statistics: residual standard error, 0.1867 on 8 degrees of freedom; multiple R^2, 0.9535; F-statistic, 18.24 on 9 and 8 degrees of freedom, the *p*-value is 0.0002056.

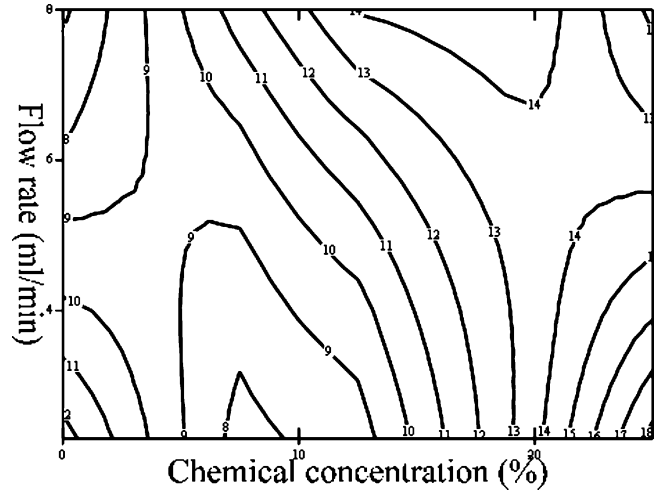

FIGURE 5. Contour chart relative oxygen concentration as a function of chemical concentration and flow rate (eq 6 at $x_1 = 0$).

CONCLUSIONS

The performance of the AtmaP surface treatment process on the surface of PP was characterized using an experimental design method, in addition to XPS and ToF-SIMS analysis. The XPS results showed a significant oxygen and nitrogen relative atomic concentration on the treated surfaces as a result of the ATmaP process. Higher oxygen flow rate with intermediate values for chemical concentration and fluid flow rates resulted in the highest experimental relative oxygen concentration on the surface. PCA collected the aliphatic hydrocarbon ions variance which corresponds to the polypropylene backbone chain scission reaction as a result of the flame treatment component of ATmaP. PCA also collected information regarding the ability of ATmaP to functionalize the surface with NO, O, and N groups at various operating conditions.

REFERENCES AND NOTES

(1) Morris, H. R.; Turner, J. F.; Munro, B.; Ryntz, R. A.; Treado, P. J. *Langmuir* **1999**, *15*, 2961–2972.
(2) Jung, C. K.; Bae, I. S.; Lee, S. B.; Cho, A. H.; Shin, E. S.; Choi, S. C.; Boo, J. H. *Thin Solid Films* **2006**, *506*−*507*, 316–322.
(3) Pijpers, A. P.; Meier, R. J. *J. Electron. Spectrosc.* **2001**, *121*, 299–313.
(4) Kwon, O. J.; Myung, S. W.; Lee, C. S.; Choi, H. S. *J. Colloid Interface Sci.* **2006**, *295*, 409–416.
(5) Lawniczak, J.; Callahan, M. *Fifth International Coatings for Plastics Symposium*; Troy, MI, May 20−22, 2002; Paint & Coatings Industry: Troy, MI, 2002.
(6) Sutherland, I.; Brewis, D. M.; Health, R. J.; Sheng, E. *Surf. Interface Anal.* **1991**, *17*, 507–510.
(7) Awaja, F.; Gilbert, M.; Kelly, G.; Fox, B.; Brynolf, R.; Pigram, P. *Surf. Interface Anal.* **2008**, *40*, 1454–1462.
(8) Lee, N.; Jang, J. *Compos. Sci. Technol.* **1998**, *57*, 1559–1569.
(9) Miller, A. C.; Berg, J. C. *Compos., Part A* **2003**, *34*, 327–332.
(10) Zhang, C. H.; Yang, F. L.; Wang, W. J.; Chen, B. *Sep. Purif. Technol.* **2007**, *61*, 276–286.
(11) Liu, Z. M.; Xu, Z. K.; Wan, L. S.; Wu, J.; Ulbricht, M. *J. Membr. Sci.* **2005**, *249*, 21–31.
(12) Sharpe, L. H. Interfaces, Interphases, and Adhesion: A Perspective. In *The Interfacial Interactions in Polymeric Composites: Proceedings of the NATO Advanced Study Institute*; Antalya/Kemer, Turkey, June 15−26, 1992; NATO Science Series E, Applied Sciences; Kluwer: Dordrecht, The Netherlands, 1993; pp 1−20.
(13) Wagner, M. S.; Graham, D. J.; Ratner, B. D.; Castner, D. G. *Surf. Sci.* **2004**, *570*, 78–97.
(14) Graham, D. J.; Wagner, M. S.; Castner, D. G. *Appl. Surf. Sci.* **2006**, *252*6860–6868.
(15) Gradowski, M.; Jacoby, T. B.; Hilgers, H.; Barz., J.; Wahl, M.; Kopnarski, M. *Surf. Coat. Technol.* **2005**, *200*, 334–340.
(16) Gardella, J. A., Jr.; Mahoney, C. M. *Appl. Surf. Sci.* **2004**, *231*−*232*, 283–288.
(17) Oran, U.; Nveren, E. U.; Wirth, T.; Unger, W. E. S. *Appl. Surf. Sci.* **2004**, *227*, 318–324.
(18) Gradowski, M.; Wahl, M.; Forch, R.; Hilgers, H. *Surf. Interface Anal.* **2004**, *36*, 1114–1118.
(19) Wagner, M. S.; Shen, M.; Horbett, T. A.; Castner, D. G. *J. Biomed. Mater. Res., A* **2003**, *64*, 1–11.
(20) Wagner, M. S.; Pasche, S.; Castner, D. G.; Textor, M. *Anal. Chem.* **2004**, *76*, 1483–1492.
(21) Me'dard, N.; Aouinti, M.; Poncin-Epaillard, F.; Bertrand, P. *Surf. Interface Anal.* **2001**, *31*, 1042–1047.
(22) Awaja, F.; Gilbert, M.; Kelly, G.; Fox, B.; Brynolf, R.; Pigram, P. J. *Surf. Interface Anal.* **2008**, *40*, 1454–1462.
(23) Cochran, W. G.; Cox, G. M. *Experimental Design*; John Wiley & Sons: New York, 1957.
(24) Mutel, B.; Grimblot, J.; Dessaux, O.; Goudmand, P. *Surf Interface Sci* **2000**, *30*, 401–406.
(25) Galuska, A. A. *Surf. Interface Anal.* **1997**, *25*, 790–798.
(26) Tomasetti, E.; Nysten, B.; Rouxhet, P. G.; Poleunis, C.; Bertrand, P.; Legras, R. *Surf. Interface Anal.* **1999**, *27*, 735–742.
(27) Lianos, L.; Quet', C.; Due, T. M. *Surf. Interface Anal.* **1994**, *21*, 14–22.
(28) Martens, H.; Naes, T. *Multivariate Calibration*; Wiley: London, 1989.
(29) Garbassi, F.; Occhiello, E. *J. Mater. Sci.* **1987**, *22*, 207–212.

AM1001376